

Efficient transfer of metallophosphor excitons via confined polaritons in organic nanocrystals

Wenbin Lu(芦文斌), Yongcong Chen(陈永聪), Xuyun Yang(杨旭云), and Ping Ao(敖平)
Citation: Chin. Phys. B, 2023, 32 (**10**): 104212. DOI: 10.1088/1674-1056/acf03b
Journal homepage: http://cpb.iphy.ac.cn; http://iopscience.iop.org/cpb

What follows is a list of articles you may be interested in

Principle of subtraction ghost imaging in scattering medium

Qin Fu(付芹), Yanfeng Bai(白艳锋), Wei Tan(谭威), Xianwei Huang(黄贤伟), Suqin Nan(南苏琴), and Xiquan Fu(傅喜泉)
Chin. Phys. B, 2023, 32 (**6**): 064203. DOI: 10.1088/1674-1056/acb202

Tunable magnomechanically induced transparency and fast-slow light in a hybrid cavity magnomechanical system

Qinghong Liao(廖庆洪), Kun Peng(彭坤), and Haiyan Qiu(邱海燕)
Chin. Phys. B, 2023, 32 (**5**): 054205. DOI: 10.1088/1674-1056/acaf2b

Tunable phonon-atom interaction in a hybrid optomechanical system

Yao Li(李耀), Chuang Li(李闯), Jiandong Zhang(张建东), Ying Dong(董莹), and Huizhu Hu(胡慧珠)
Chin. Phys. B, 2023, 32 (**4**): 044213. DOI: 10.1088/1674-1056/acb9ea

Effective dynamics and quantum state engineering by periodic kicks

Zhi-Cheng Shi(施志成), Zhen Chen(陈阵), Jian-Hui Wang(王建辉), Yan Xia(夏岩), and X X Yi(衣学喜)
Chin. Phys. B, 2023, 32 (**4**): 044210. DOI: 10.1088/1674-1056/ac7bfc

Light manipulation by dual channel storage in ultra-cold Rydberg medium

Xue-Dong Tian(田雪冬), Zi-Jiao Jing(景梓骄), Feng-Zhen Lv(吕凤珍),Qian-Qian Bao(鲍倩倩), and Yi-Mou Liu(刘一谋)
Chin. Phys. B, 2023, 32 (**4**): 044205. DOI: 10.1088/1674-1056/ac946c

---

Efficient transfer of metallophosphor excitons via confined polaritons in organic nanocrystals

Wenbin Lu(芦文斌)[1], Yongcong Chen(陈永聪)[1,†], Xuyun Yang(杨旭云)[1], and Ping Ao(敖平)[2]

[1] *Shanghai Center for Quantitative Life Sciences & Physics Department, Shanghai University, Shanghai* 200444, *China*
[2] *College of Biomedical Engineering, Sichuan University, Sichuan* 610064, *China*

(Received 7 June 2023; revised manuscript received 8 August 2023; accepted manuscript online 15 August 2023)

We investigate the transfer of phosphorescent energy between co-assembled metallophosphors in crystalline nanostructures [*Angew. Chem. Int. Ed.* **57** 7820 (2018) and *J. Am. Chem. Soc.* **140** 4269 (2018)]. Neither Dexter's nor Förster's mechanism of resonance energy transfer (RET) could account fully for the observed rates, which exceed 85% with significant temperature dependence. But there exists an alternative pathway on RET mediated by intermediate states of resonantly confined exciton–polaritons. Such a mechanism was used to analyze artificial photosynthesis in organic fluorescents [*Phys. Rev. Lett.* **122** 257402 (2019)]. For metallophosphors, the confined modes act as extended states lying between the molecular S_1 and T_1 states, offering a bridge for the long-lived T_1 excitons to migrate from donors to acceptors. Population dynamics with parameters taken entirely based on experiments fits the observed lifetimes of phosphorescence across a broad range of doping and temperature.

Keywords: organic nanocrystals, phosphorescent emission, resonance energy transfer, exciton–polariton

PACS: 42.50.–p, 03.65.–w, 62.23.St **DOI:** 10.1088/1674-1056/acf03b

1. Introduction

Artificial light-harvesting systems of organic self-assembled crystals have attracted considerable research interests due to their potential applications in solar energy and micro electronics.[1–3] Inspired by the ultra-high efficient energy transfer (over 95%) in natural plants and photosynthetic bacteria, the light-harvesting nanocrystal systems, including those assembled by transition metal with different ligands, have been extensively studied.[4–6] Vast numbers of light-absorbing antennas (donors) and rapid transfer of excitations to a small number of acceptors are the key features observed in these systems. High degree of spatial organization and appropriate energy gradient appear conducive to the efficient transfer.[7] Specific cases of energy transfer between two fluorescent molecules[8,9] or between fluorescent donor and phosphorescent acceptor have been frequently explored.[10–12] Nevertheless, some fundamental questions regarding the energy transfer between two phosphorescent molecules remain elusive.[13]

We focus in this work on the reported energy transfer between two transition-metal complexes in nanocrystals. (i) Light-harvesting nanorods are from coassembly of iridium (Ir) and ruthenium (Ru) metallophosphors.[7] The crystals of $[Ir(ppy)_2(pzpy)](PF_6)$ (Ir donor) have smooth surface and uniform size. The emission spectrum is predominated by doped $[Ru(bpy)_3](PF_6)_2$ (Ru acceptor) when the doping ratio reaches 1.5%, resulting in 90% quenching of the Ir-donor's emission. (ii) Thermal-responsive phosphorescent nanotubes are from coassembly of two Ir complexes $[Ir(dmppy)_3]$ (Ir-D) and $[Ir(piq)_3]$ (Ir-A).[14] Again, when the concentration of Ir-A saturates at 0.5%, 85% of the energy is transferred.

Neither Dexter electron exchange nor Förster resonance energy transfer (FRET) mechanism is able to fully account for the observed transfer rates in the experiments. A spherical model that mimics the crystal packing of the Ir donor complexes around the Ru center was used in Ref. [7]. Their analysis concluded that the short-range of the T_1–T_1 Dexter mechanism alone could not account for the high efficiency when the A/D ratio $> 1/100$. Furthermore, the T_1–S_1 FRET rate from donor to acceptor, which is characterized by the Coulombic dipole–dipole interaction and can be related to the radiative decay rate of the molecules, would only drop by roughly a factor of 2, while the rate constant obtained from the lifetime decay measurement dropped more than ten folds in the second experiment from 298 K to 118 K.[14]

We propose an alternative energy transfer pathway that is mediated by resonance-confined polaritons in this work. Note that the natural boundaries of a nanocrystal provide a microcavity of resonance for the lights emitted from the donors. They can be confined within the cavity as exciton–polaritons (EPs) to facilitate the energy transfer. A previous study showed that delocalized EPs could lead to ultra-efficient ($> 90\%$) S_1–S_1 energy transfer at less than 1/1000 of doping ratio.[15,16] In the current context, the presence of transition metal elements such as Ir or Ru makes the T_1 state of the organic complexes the lowest visible excitation via intersystem crossing. There arises complex inter-plays and population dynamics among the S_1, T_1 and the EP states. The energy transfer can then occur via the route (donor) $T_1 \rightarrow S_1 \rightarrow$

†Corresponding author. E-mail: chenyongcong@shu.edu.cn

© 2023 Chinese Physical Society and IOP Publishing Ltd

EP states → (acceptor)S_1 → T_1 → emission. Our analysis is able to account quantitatively, with no fitting parameters, for the observed dependence of the donor's phosphorescent lifetime with temperature and doping ratio.

This work is organized as follows. In Section 2, we describe the core process of the proposed mechanism, starting with the resonance inside the micron-scale crystal and quantization of the electromagnetic (EM) fields. We show explicitly how EPs as composite entities mediate the energy transfer between the S_1 states of donors and acceptors. Then in Section 3, a population dynamics engaging the T_1-excitons is formulated for a quantitative study of the donor's decay process. In Section 4 we turn to the primary subject of this study, applying the theory to both the Ir–Ru metallophosphor binary and the Ir–Ir donor–acceptor nanocrystals. The final section (Section 5) summarises the main findings with a perspective on further exploration of EPs in the context of resonance energy transfer (RET).

2. Polariton-mediated RET process

2.1. Resonance inside the micron-scale crystal

We first present a brief review of a previous study[16] in which the standing EM waves are sustained by the natural boundaries of a nanocrystal. The micron-scale crystal dimensions are crucial for the confinement of EPs formed as a result of strong coupling between the EM field and localized S_1 exictons of the molecules. The resonant modes become captive under total internal reflections. To exemplify the concept, we take for simplicity and with no loss of generality that the nanocrystal is a rectangular isotropic dielectric medium of dimensions $L_1 \times L_2 \times L_3$. Let

$$\boldsymbol{E}(\boldsymbol{r},t) = \boldsymbol{U}_{\boldsymbol{k}\alpha}(\boldsymbol{r})\cos(\omega_{\boldsymbol{k}}t),\ \ \varepsilon_{\rm b}\omega_{\boldsymbol{k}}^2 = \boldsymbol{k}^2c^2, \tag{1}$$

where the electric field inside the cavity under background relative permittivity $\varepsilon_{\rm b}$ that excludes specifically the contribution from the excitons. Following Ref. [16], $\boldsymbol{U}_{\boldsymbol{k}\alpha}(\boldsymbol{r})$ is a superposition of plane waves taking the form of[17–19]

$$\begin{aligned}&\boldsymbol{U}_{\boldsymbol{k}\alpha}(\boldsymbol{r}) = (u_{x\boldsymbol{k}\alpha}U_{x\boldsymbol{k}}(\boldsymbol{r}), u_{y\boldsymbol{k}\alpha}U_{y\boldsymbol{k}}(\boldsymbol{r}), u_{z\boldsymbol{k}\alpha}U_{z\boldsymbol{k}}(\boldsymbol{r})),\\ &\boldsymbol{u}_{\boldsymbol{k}\alpha} = (u_{x\boldsymbol{k}\alpha}, u_{y\boldsymbol{k}\alpha}, u_{z\boldsymbol{k}\alpha}),\ \ \alpha = 1,2,\end{aligned} \tag{2}$$

where $\boldsymbol{u}_{\boldsymbol{k}\alpha}$ are the two polarization vectors and the wave vector $\boldsymbol{k} = (k_x, k_y, k_z)$ is limited to the first octant

$$\begin{aligned}&\boldsymbol{k} = (\pi l_1/L_1, \pi l_2/L_2, \pi l_3/L_3),\ \ l_i = 0,1,2,3,\ldots\\ &\tilde{\boldsymbol{k}} = \boldsymbol{k}/|\boldsymbol{k}| = \boldsymbol{u}_{\boldsymbol{k}1}\times\boldsymbol{u}_{\boldsymbol{k}2},\ \ \boldsymbol{u}_{\boldsymbol{k}\alpha}\cdot\boldsymbol{u}_{\boldsymbol{k}\alpha'} = \delta_{\alpha\alpha'}.\end{aligned} \tag{3}$$

A wave is trapped inside when the tangent component of the wave vector

$$\boldsymbol{k}_\parallel^2c^2 > \varepsilon_{\rm s}(E_{\boldsymbol{k}}/\hbar)^2 \tag{4}$$

holds on all the surfaces, more explicitly $\boldsymbol{k}_\parallel^2 = (k_x^2+k_y^2), (k_y^2+k_z^2), (k_z^2+k_x^2)$. In the above, $\varepsilon_{\rm s}$ is the dielectric constant of the surrounding medium and $E_{\boldsymbol{k}}$ is the lower-branch energy of EP to be shown below.

2.2. Quantization of the EM wave and S_1-exciton

For quantum mechanical modeling of EM interaction with the S_1 excitons, one can quantize the macroscopic Maxwell equations using above eigenmodes. On a given $\boldsymbol{k}$, the photon Hamiltonian and the electric field operator inside the cavity are given by (see Ref. [20])

$$\hat{H}_{{\rm p}\boldsymbol{k}} = \sum_\alpha \hbar\omega_{\boldsymbol{k}}(\hat{a}_{\boldsymbol{k}\alpha}^\dagger\hat{a}_{\boldsymbol{k}\alpha} + \frac{1}{2}), \tag{5}$$

$$\hat{\mathcal{E}}_{\boldsymbol{k}}(\boldsymbol{r}) = \sum_\alpha f_{\boldsymbol{k}}(\hat{a}_{\boldsymbol{k}\alpha} + \hat{a}_{\boldsymbol{k}\alpha}^\dagger)\boldsymbol{U}_{\boldsymbol{k}\alpha}(\boldsymbol{r}), \tag{6}$$

where $f_{\boldsymbol{k}} = \sqrt{\hbar\omega_{\boldsymbol{k}}/(2\varepsilon_0\varepsilon_{\rm b})}$ and the phase of $\hat{a}_{\boldsymbol{k}\alpha}$ are chosen for symmetric $\hat{\mathcal{E}}_{\boldsymbol{k}}(\boldsymbol{r})$.

As for the exciton, we can approximate it by a harmonic oscillator that is restricted to its zeroth and first levels, namely the one excitation manifold. The position of the j-th molecule is $\boldsymbol{R}_j$, the creation and annihilation operators of the oscillator are $\hat{b}_j^\dagger$ and $\hat{b}_j$, respectively, and the dipole matrix element between the ground and the excited states is $\boldsymbol{d} = \langle g|\hat{\boldsymbol{r}}|e\rangle$, we have the exciton–photon interaction Hamiltonian

$$\begin{aligned}&\hat{H}_{{\rm l}\boldsymbol{k}} = \sum_{j,\alpha} ef_{\boldsymbol{k}}\left[\boldsymbol{U}_{\boldsymbol{k}\alpha}(\boldsymbol{R}_j)\cdot(\boldsymbol{d}^*\hat{b}_j^\dagger\hat{a}_{\boldsymbol{k}\alpha} + \boldsymbol{d}\hat{a}_{\boldsymbol{k}\alpha}^\dagger\hat{b}_j)\right],\\ &[\hat{b}_i, \hat{b}_j^\dagger] = \delta_{ij},\ \ i,j = 1,2,\cdots,N.\end{aligned} \tag{7}$$

Note that in a self-assembled narocrystal, $\boldsymbol{R}_j$ form a crystalline lattice of N molecules. We can further take all molecules with the identical matrix element, i.e., ignoring the orientation difference between the different groups of molecules in the crystal.

Similar to Ref. [21], we can construct a standing-wave (SW) superposition of the identical S_1 states from all the molecules

$$\hat{b}_{z\boldsymbol{k}}^\dagger = \sqrt{\frac{V}{N}}\sum_j\left[U_{z\boldsymbol{k}}(\boldsymbol{R}_j)\hat{b}_j^\dagger\right], \tag{8}$$

$$|\phi_{z\boldsymbol{k}}\rangle = \hat{b}_{z\boldsymbol{k}}^\dagger|0\rangle,\ \ [\hat{b}_{z\boldsymbol{k}}, \hat{b}_{z\boldsymbol{k}}^\dagger] = 1. \tag{9}$$

Two more SW states $|\phi_{x\boldsymbol{k}}\rangle$ and $|\phi_{y\boldsymbol{k}}\rangle$ can be likewise defined respectively for the x and y components. The three SW states are mutually orthogonal for a given $\boldsymbol{k}$ (for large N). More details can be found in part A of the supplementary information (SI)[19] of this work.

2.3. Polariton as a S_1-exciton–photon composite

The total Hamiltonian under Eq. (8), which includes the photon Hamiltonian, the exciton Hamiltonian and the interactive Hamiltonian between them, reads

$$\hat{H} = \sum_{\gamma}\hbar\omega_{\rm e}\hat{b}^{\dagger}_{\gamma\boldsymbol{k}}\hat{b}_{\gamma\boldsymbol{k}} + \sum_{\alpha}\hbar\omega_{\boldsymbol{k}}\hat{a}^{\dagger}_{\boldsymbol{k}\alpha}\hat{a}_{\boldsymbol{k}\alpha} + \sum_{\gamma,\alpha}\left[g_{\boldsymbol{k}}\tilde{\boldsymbol{d}}^{*}_{\gamma}\cdot\boldsymbol{u}_{\boldsymbol{k}\alpha}\hat{b}^{\dagger}_{\gamma\boldsymbol{k}}\hat{a}_{\boldsymbol{k}\alpha} + g_{\boldsymbol{k}}\tilde{\boldsymbol{d}}_{\gamma}\cdot\boldsymbol{u}^{*}_{\boldsymbol{k}\alpha}\hat{a}^{\dagger}_{\boldsymbol{k}\alpha}\hat{b}_{\gamma\boldsymbol{k}}\right]. \quad (10)$$

In the above, $g_{\boldsymbol{k}} = e|\boldsymbol{d}|f_{\boldsymbol{k}}\sqrt{N/V}$ measured the coupling strength of the cavity EM mode and the excitons and $\tilde{\boldsymbol{d}}_{\gamma} = \boldsymbol{d}_{\gamma}/|\boldsymbol{d}|$ ($\gamma = x,y,z$) is a dimensionless unit vector of the dipole moment. The Hamiltonian of Eq. (10) can be diagonalized for the dispersion of the combined entity. Let $\Delta E_{\boldsymbol{k}} = \hbar\omega_{\rm e} - E_{\boldsymbol{k}}$ be the lower-branch energy drop of the resulting EP and consider a simple isotropic scenario $|\tilde{\boldsymbol{d}}_{\gamma}| = 1/\sqrt{3}$, we obtain

$$\Delta E_{\boldsymbol{k}} = \sqrt{\frac{(\hbar\Omega_{\boldsymbol{k}})^2}{4} + \frac{g^2_{\boldsymbol{k}}}{3}} - \frac{\hbar\Omega_{\boldsymbol{k}}}{2}, \quad (11)$$

where the photon–exciton frequency detuning is $\hbar\Omega_{\boldsymbol{k}} = \hbar\omega_{\boldsymbol{k}} - \hbar\omega_{\rm e}$.

Knowledge of $E_{\boldsymbol{k}}$ can be used in Eq. (4) to determine the modes that are confined by the natural boundaries of the crystal. Details relevant to the two experiments considered in this work are presented in part C of SI.[19] The results show that the majority of EPs emitted from the donor's S_1 state are indeed trapped in the cavity. Such a characteristic is assumed throughout the rest of this work.

2.4. Transition rate to acceptor S_1 state

The transition from a trapped EP state to the doped acceptors is enabled by a small photonic component $A_{\rm ph} \leq 20\%$ in the EP entity. We can calculate the transition rate via the Fermi golden based on the component. For further details, cf. part C of SI.[19] For an EP in $\boldsymbol{k}_{\alpha}$ mode, the rate reads

$$\Gamma_{\rm ac} \approx \frac{2\pi A_{\rm ph}}{3}\left(\frac{g_{\boldsymbol{k}}}{\hbar\omega_{\rm e}}\right)^2\left(\frac{\omega_{\rm e}}{\Delta\omega}\right)\omega_{\rm e}\times\frac{N_{\rm a}}{N} \approx \Gamma_0\times\frac{N_{\rm a}}{N}, \quad (12)$$

where $N_{\rm a}/N$ is the doping ratio of acceptors evenly distributed in the crystal with a spectral bandwidth $\Delta\omega$ roughly $\omega_{\rm e}/\Delta\omega \approx 10$. It turns out $\Gamma_0 \approx \omega_{\rm e}$.

3. Population of T_1, S_1 and EP states

We next study the interplay between the T_1, S_1 and the EP states that are engaged in the energy transfer process. Figure 1(a) presents a Jablonski diagram of these states, also depicts the virtual levels of Stokes shift ($\hbar\omega_{\rm s}$) associated with radiation. They appear in the vertical transition picture for absorption and emission. The first absorption peak corresponds to the donor's energy of $S_1 + \hbar\omega_{\rm s}$. The phosphorescent emission occurs at that of $T_1 - \hbar\omega_{\rm s}$. We can infer the intrinsic energy difference between T_1 and S_1 states $\Delta E_{\rm TS}$ from the measured difference between the two peaks, with the subtraction of $2\hbar\omega_{\rm s}$. In addition, the fluorescent emission of S_1 exciton into an EP state is accompanied by an energy drop of $\hbar\omega_{\rm s}$. We will later identify the energy difference between T_1 and EP as the activation energy $E_{\rm a}$ that dictates the temperature dependence of the energy transfer from donor to acceptor. We obtain $\Delta E_{\rm TS} = \hbar\omega_{\rm s} + E_{\rm a}$ as shown in the figure. Finally, $\Delta E_{\boldsymbol{k}}$ in Eq. (11) is actually $\approx 2\hbar\omega_{\rm s}$, as $\hbar\omega_{\rm e}$ should be raised by $\hbar\omega_{\rm s}$ itself.[16]

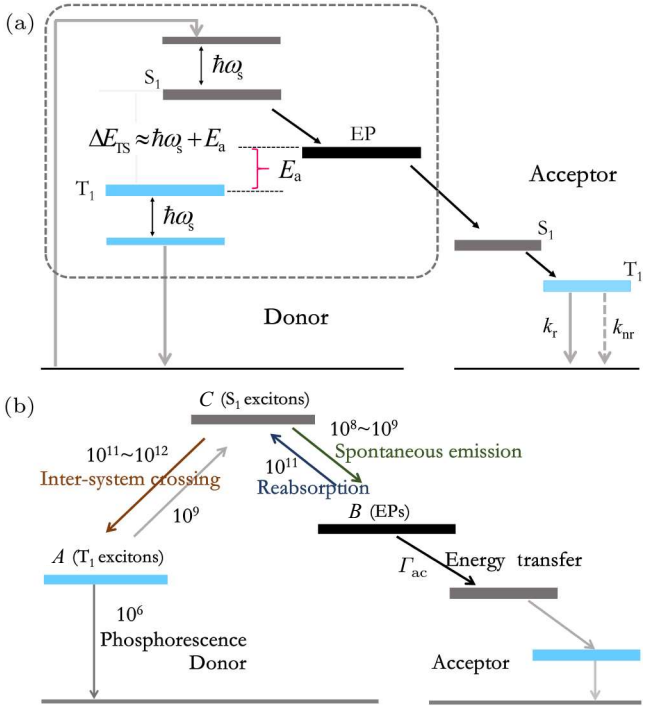


Fig. 1. (a) Jablonski diagram for the states of S_1, T_1 and EPs along with Stokes shift of $\pm\hbar\omega_{\rm s}$ for absorption/emission process. $\Delta E_{\rm TS} \approx \hbar\omega_{\rm s} + E_{\rm a}$ with $E_{\rm a} \approx 0$ for the Ir–Ru and $E_{\rm a} \approx 0.04$ eV for the thermal-responsive phosphorescent Ir–Ir system. (b) Transitions between different energy levels and typical values for the rates. Their population dynamics sets the transfer rate from T_1 to T_1 of donor to acceptor.

To proceed further, let us denote the time-dependent ensemble population of T_1 excitons as $A(t)$, that of EPs as $B(t)$, and S_1 as $C(t)$. The possible transition paths between them are shown in Fig. 1(b). Their time evolution can be expressed as

$$\begin{aligned}\dot{A}(t) &= k_{\rm ST}C(t) - (k_{\rm P} + k_{\rm TS})A(t),\\ \dot{B}(t) &= k_{\rm F}C(t) - (\Gamma_{\rm re} + \Gamma_{\rm ac})B(t),\\ \dot{C}(t) &= -(k_{\rm ST} + k_{\rm F})C(t) + \Gamma_{\rm re}B(t) + k_{\rm TS}A(t). \end{aligned} \quad (13)$$

In the above, the parameters are associated with the following physical processes. $k_{\rm ST} \approx 10^{11}$–$10^{12}$ s^{-1} stands for the fast inter-system crossing from S_1 to T_1. While $k_{\rm TS} \approx 10^{9}$ s^{-1} is for the reverse, which is temperature dependent and suppressed by the $\Delta E_{\rm TS}$ energy barrier. $k_{\rm P} \approx 10^{6}$ s^{-1} is the total decay rate of T_1 that includes phosphorescence. $k_{\rm F} \approx 10^{9}$ s^{-1}

is the fluorescence emission rate from S_1 to EP. The later can either return to S_1 or go down to an acceptor (completing energy transfer). $\Gamma_{re} \approx 10^{11}$–$10^{12}$ s^{-1} indicates the rate for the reabsorption process. It can be higher than k_P due to the vast number of donor molecules that compete against the relative minor energy drop. Finally, Γ_{ac} is given by Eq. (12) scales with the doping ratio.

One can deduct an overall process of exciton migration based on the rate magnitudes as shown in Fig. 1(b). An exciton created by UV radiation would quickly reach the T_1 state of a donor from S_1 via inter-system crossing, assisted by spin–orbit coupling in the metallophosphor. It would do roughly $k_{TS}/k_P \sim 10^3$ round-trips to the S_1 during its life time. But there is a small probability $k_F/k_{ST} \sim 10^{-2}$ that would detour to an EP state, about ~ 10 times, setting a saturation limit of $\sim 90\%$ efficiency. While at the later, it would have either returned to S_1 or be captured by an acceptor, depending on the relative ratio of Γ_{re} vs. Γ_{ac}. Equation (12) for Γ_{ac} would then give rise to significant portion of transfer at relative low doping ratio of $\sim 10^{-4}$. In the absence of doping, there would sustain a quasi steady distribution with a Boltzmann-like energy factor relating A and B, as both $A \to C$ and $B \to C$ would rely on thermo-activation over energy deficit. The Boltzmann factor would correspond to the observed temperature dependence observed on the Ir–Ir system. More detailed analyses below confirm this gross picture.

4. Experiments and analysis

4.1. Nanorods of Ir–Ru metallophosphors

The first system comprises a donor–acceptor arrangement achieved via the coassembly of two polypyridyl metallophosphors, namely Ir and Ru, which function as the antenna chromophore and the energy acceptor respectively. The nanorods exhibit multicolor phosphorescence due to efficient S_1 to T_1 inter-system crossing in the presence of Ir element (transition metal). These rods have a uniform size and smooth surface. The Ir donor possesses a T_1 energy of 2.61 eV (by emission), which is lower than the S_1 energy of 2.82 eV (by absorption). Notably, the brighter emission at the two ends of nanorods displays color-tunable optical waveguide characteristics, which supports the core point of EP confinement used in this work.

The exciton–photon interaction depends on the crystallographic and spectroscopic characteristics of the S_1 state. The dipole moment of the $Ir(ppy)_2(pzpy)$ donor molecule can be estimated to be approximately 6.4 D (Debyes), which corresponds to $|\boldsymbol{d}| \approx 1.3$ Å based on the integral of extinction coefficient over the absorption frequencies (see Refs. [22,23] and part B of SI[19]). A unit cell of the crystal contains 8 donor molecules with a volume of 5636 Å^3 (Table S1 in Ref. [7]). Part C of SI[19] has the details regarding the formation of EP states facilitated by the resonance-confined EM waves. At the resonance level $\hbar\omega_e = \hbar\omega_{\boldsymbol{k}} \approx 2.82$ eV, the coupling constant $g_{\boldsymbol{k}} \approx 0.56$ eV.

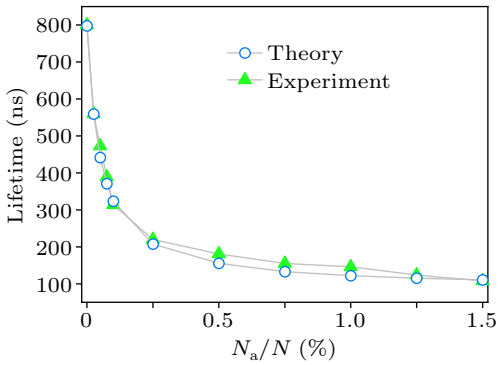


Fig. 2. The dependence of the lifetime of the Ir donor on N_a/N of the doped $[Ru(bpy)_3](PF_6)_2$ in $[Ir(ppy)_2(pzpy)](PF_6)$ crystal. Open cycles (blue) are the theoretical curve with no fitting parameter, cf. part C of SI.[19] Solid triangles (green) are the experimental data taken from Table S4 of SI in Ref. [7].

The lifetime of the Ir donors descends from 800 ns to 108 ns as the doping of the Ru acceptors rises from 0 to 1.5%. Numerical results of Eq. (13), using parameters derived from the experimental data (cf. Table S4 of Ref. [7]) as summarized in Table S2 of SI,[19] are shown in Fig. 2 alongside the experimental ones. The overall match is excellent. At zero doping, the lifetime of T_1 exciton is 798 ns vs. 800 ns. The agreement goes all the way to the saturated doping of 1.5% where the theoretical value is 110 ns vs. the observed lifetime of 108 ns.

4.2. Thermal-responsive Ir–Ir tubes

The second set of experiment is on thermal phosphorescent $[Ir(dmppy)_3]$ nanotubes which were fabricated with the ability to display color-tunable phosphorescence. The doping of $[Ir(piq)_3]$ is adjusted from 0 to 0.5% and the temperature is within the range 298 K to 77 K. Upon exposure to UV radiation, the tips of these nanotubes exhibit brighter emissions compared to the body section, indicating again the presence of an active optical waveguide. Although the tubes have a smooth hexagonal outer shape in general, we use a similar size of the rectangular waveguide and assume the polarization of the molecules aligned to a fixed orientation (see part C of SI[19]) to simplify the modeling work.

The high extinction coefficient on the tubes yields a dipole moment of 8 D (see part B of SI[19]). The crystal contains 6 molecules in a unit cell with a size of 4491 Å^3, and S_1 state of the metallophosphor has $\hbar\omega_e = 2.72$ eV (by absorption). For completeness, the T_1 state emits at 2.43 eV. The confined EP modes are studied in part C in Ref. [19]. We obtain the coupling constant $g_{\boldsymbol{k}} \approx 0.61$ eV (at $\hbar\omega_{\boldsymbol{k}} = \hbar\omega_e$).

Figure 3(a) shows the dependence of the phosphorescent lifetime of $[Ir(dmppy)_3]$ on the doping ratio N_a/N of $[Ir(piq)_3]$ spanned from 0 to 0.15%. The comparison substantiates a high degree of agreement between the theoretical results and

the experimental data obtained from Table S3 of the Supporting Information in Ref. [14]. The required parameters for the calculation are summarized in Table S2 of SI[19] and Refs. [24–29]. The slight discrepancy at the larger doping end might be attributed to the inadequate etching by poor solvents that caused non-penetrated morphology of hollow structures. This could add extra decays not included in our theoretical model. Furthermore, the resonant confinement of EPs under a closer shape, such as cylindrical symmetry should be further explored.

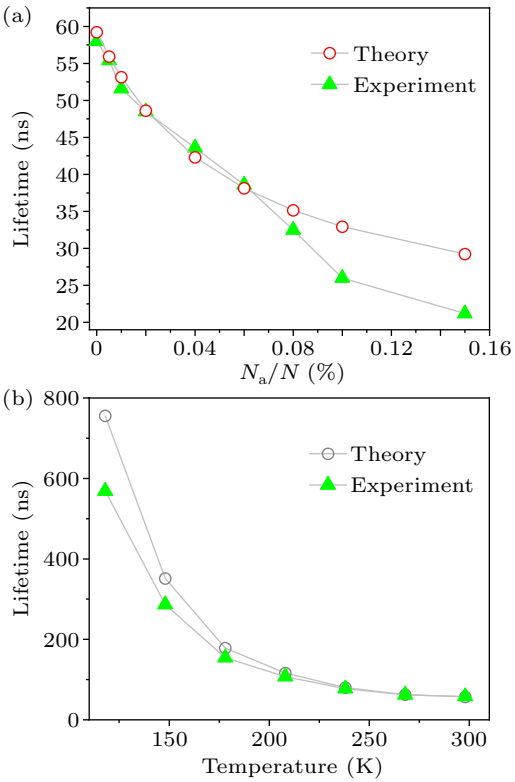


Fig. 3. (a) Room-temperature lifetime of $[Ir(dmppy)_3]$ metallophosphor as a function of doped ratio N_a/N of $[Ir(piq)_3]$. Theoretical results with no adjustable parameters are in open circles (red). They are plotted against the experimental ones in the solid triangle (green), taken from Table S3 of support information in Ref. [14]. (b) The temperature dependence of lifetime, with an activation energy of 40 meV as a result of the difference between the T_1 and the EP levels. Theoretical predictions in open circles (grey) are drawn alongside the experimental data at $N_a/N = 0.06\%$.

Unlike the first experiment, the lifetime has a significant dependence on temperature. Arrhenius fitting of experimental data reveals an activation energy of $E_a = 40$ meV. In the population dynamics outlined above, such barrier can be naturally attributed to the difference between the T_1 and the EP states. Namely, it is the balancing result between the reverse inter-system crossing (cf. k_{TS}) and the reabsorption (Γ_{re}) to the donor's S_1 state at the top. These parameters are given in Table S1 of SI[19] and Refs. [27,30]. Figure 3(b) shows that the theoretical calculations are in excellent agreement with the experimental results. Explicitly, it predicts a lifetime of roughly 550 ns even at 118 K (with 0.06% doping), which matches the experimental observation of 570 ns.

5. Discussion

We have assumed that there are adequate number of EP modes near the S_1 emission spectrum. But in reality, the assumption can become an issue as it would depend on the geometry and dimensions of the nanocrystal in question. It would be interesting for such dependence to be taken into account in both theoretical and experimental works in the future. There are also minor mismatches between the theory and experiment in Fig. 3. While the discrepancy at the higher doping levels might be caused by material quality control with experiment, the deviation at the low-temperature end is likely due to some overestimate of the activation energy E_a from the Arrhenius equation, cf. Fig. 1. In the latter case, the activation rate (from T_1 to S_1) is more sensitive to the energy difference as the temperature decreases.

To summarize, we present an alternative explanation for the efficient transfer of metallophosphor (T_1) excitons in organic nanocrystals observed in Refs. [7,14]. The proposed mechanism focuses on the intermediate states of exciton–polaritons. We first show that these EPs can be trapped by the natural boundaries of the crystal.[16] Then a population dynamics involving T_1, S_1 and the confined EPs is formulated with various transition parameters taken or deducted entirely from known experimental data. The results on the phosphorescent lifetime of the metallophosphors are in excellent agreement with that from experiments. Theoretical predictions match experimental curves over a wide range of doping concentrations and temperatures. In particular, the temperature dependence is shown to arise from the energy difference between the T_1 and the EP states, which is much smaller than that between the T_1 and S_1 states. The success of the theory may be of significance to the applications of these materials in miniaturized photonic devices and solar energy harvesting.[31,32] Finally, we hope more experiments with regard to the mechanism can be conducted in future studies.

Acknowledgments

Project supported by the National Natural Science Foundation of China (Grant No. 16Z103060007) (PA). One of us (YCC) thanks Prof. Y W Zhong for visiting Shanghai University and for an insightful discussion on the experimental works. Thanks Shanghai Nanobubble Technology Co., Ltd. for supporting this work.

References

[1] Korotkevich A O, Galochkina Z S, Lavrova O and Coutsias E A 2015 *Renew. Energ.* **81** 804
[2] Creatore C, Chin A W, Parker M A and Emmott S 2015 *Front. Mater.* **2** 6
[3] Panda M K, Ladomenou K and Coutsolelos A G 2012 *Coord. Chem. Rev.* **256** 2601
[4] van Grondelle R, Dekker J P, Gillbro T and Sundstrom V 1994 *Biochimica et Biophysica Acta (BBA)-Bioenergetics* **1187** 1

[5] Brooks J, Babayan Y, Lamansky S, Djurovich P I, Tsyba I, Bau R and Thompson M E 2002 *Inorg. Chem.* **41** 3055

[6] Grushin V V, Herron N, LeCloux D D, Marshall W J, Petrov V A and Wang Y 2001 *Chem. Commun.* **16** 1494

[7] Sun M J, Liu Y, Yan Y, Li R, Shi Q, Zhao Y S, Zhong Y W and Yao J 2018 *J. Am. Chem. Soc.*

[8] Berggren M, Dodabalapur A, Slusher R and Bao Z 1997 *Nature* **389** 466

[9] Morawetz H 1988 *Science* **240** 172

[10] Baldo M A, Adachi C and Forrest S R 2000 *Phys. Rev. B* **62** 10967

[11] Baldo M A, O'Brien D F, You Y, Shoustikov A, Sibley S, Thompson M E and Forrest S R 1998 *Nature* **395** 151

[12] Kalinowski J, Stampor W, Cocchi M, Virgili D, Fattori V and Di Marco P 2004 *Chem. Phys.* **297** 39

[13] Steinbacher F S, Krause R, Hunze A and Winnacker A 2012 *Phys. Status Solidi (a)* **209** 340

[14] Sun M J, Zhong Y W and Yao J 2018 *Angew. Chem. Int. Ed.* **57** 7820

[15] Chen P Z, Weng Y X, Niu L Y, Chen Y Z, Wu L Z, Tung C H and Yang Q Z 2016 *Angew. Chem. Int. Ed.* **55** 2759

[16] Chen Y C, Song B, Leggett A J, Ao P and Zhu X 2019 *Phys. Rev. Lett.* **122** 257402

[17] Morse P M and Feshbach H 1954 *Am. J. Phys.* **22** 410

[18] Dicke R H 1954 *Phys. Rev.* **93** 99

[19] Lu W B, Chen Y C, Yang X Y and Ao P 2023 *Supplemental information at url will be inserted by publisher on additional algebraic works for the present work*

[20] Kakazu K and Kim Y 1994 *Phys. Rev. A* **50** 1830

[21] Pekar S 1958 *J. Phys. Chem. Solids* **5** 11

[22] Parson W W 2009 *Modern Optical Spectroscopy: With Exercises and Examples from Biophysics and Biochemistry* (Berlin: Springer)

[23] Wu S H, Ling J W, Lai S H, Huang M J, Cheng C H and Chen I C 2010 *J. Phys. Chem. A* **114** 10339

[24] Pander P, Daniels R, Zaytsev A V, Horn A, Sil A, Penfold T J, Williams J G, Kozhevnikov V N and Dias F B 2021 *Chem. Sci.* **12** 6172

[25] To W P, Zhou D, Tong G S M, Cheng G, Yang C and Che C M 2017 *Angew. Chem. Int. Ed.* **56** 14036

[26] Peng L Y, Li Z W, Pan G N, Chen W K, Gao Y J and Cui G 2023 *Phys. Chem. Chem. Phys.* **25** 6454

[27] Stranius K, Hertzog M and Börjesson K 2018 *Nat. Commun.* **9** 2273

[28] Yersin H 2008 *Highly Efficient OLEDs with Phosphorescent Materials* (Hoboken: John Wiley & Sons)

[29] Kleinschmidt M, van Wüllen C and Marian C M 2015 *J. Chem. Phys.* **142** 094301

[30] Parker C and Hatchard C 1962 *J. Phys. Chem.* **66** 2506

[31] Yan Y and Zhao Y S 2012 *Adv. Funct. Mater.* **22** 1330

[32] Liu Z, Duan G, Duan H and Wang Z 2022 *Sol. Energy Mater. Sol. Cells* **240** 111688